Highly Electron-Deficient Pyridinium-Nitrones for Rapid and Tunable Inverse-Electron-Demand Strain-Promoted Alkyne-Nitrone Cycloaddition to Bicyclo[6.1.0]nonyne

Praveen N. Gunawardene, Wilson Luo, Alexander M. Polgar, John F. Corrigan, Mark S. Workentin*

Department of Chemistry and the Centre for Materials and Biomaterials Research, *The* University *of* Western Ontario, Richmond Street, London, Ontario, Canada. E-mail: mworkent@uwo.ca; Tel: 1 519-661-2111 ext. 86319

Supporting Information Placeholder

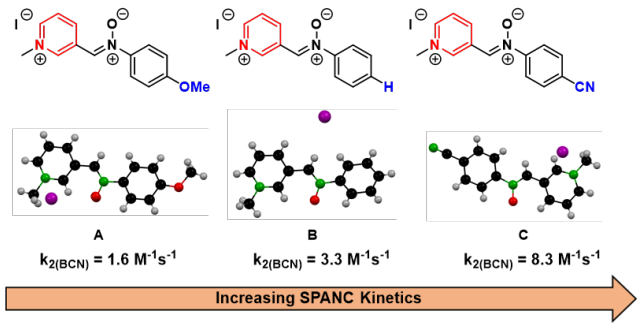

ABSTRACT: Highly accelerated inverse-electron-demand strain-promoted alkyne-nitrone cycloaddition (IED SPANC) between a stable cyclooctyne (bicyclo[6.1.0]nonyne (BCN)) and nitrones delocalized into a C_α–pyridinium functionality is reported, with the most electron-deficient "pyridinium–nitrone" displaying among the most rapid cycloadditions to BCN that is currently reported. Density functional theory (DFT) and X–ray crystallography are explored to rationalize the effects of *N*– and C_α–substituent modifications at the nitrone on IED SPANC reaction kinetics and the overall rapid reactivity of pyridinium–delocalized nitrones.

INTRODUCTION

Bimolecular strain–promoted cycloaddition reactions between cycloalkyne dipolarophiles and 1,3 dipoles are a subset of bioorthogonal 'click' reactions that have become a powerful tool in chemical biology[1–4] and nanomaterial science,[5–8] for the fusion of two complex substrates that is otherwise inaccessible. Their practicality can be largely attributed to the high chemoselectivity and non–perturbing biocompatibility of the complementary reactive partners in the presence of other reactive moieties in both natural and synthetic settings.[9,10] At the same time, they maintain high reaction kinetics compared to other bioorthogonal reactions such as the Staudinger–Bertozzi ligation and thiol–maleimide reaction.[11] First developed by Bertozzi and co–workers, the prototype variant of such strain–promoted cycloaddition is the reaction between a cyclooctyne, which is the smallest stable cycloalkyne, and an azide dipole, and is more commonly known as the strain–promoted alkyne–azide cycloaddition (SPAAC).[12] A less well–known homologous variant of SPAAC is the reaction between a cyclooctyne and nitrone dipole, and is termed the strain–promoted alkyne–nitrone cycloaddition (SPANC).[13]

In recent years, there has been a growing interest toward the acceleration of the reaction kinetics of both SPAAC and SPANC by tailoring the structure and electronic composition of the reactive partners to promote more favorable frontier orbital energy overlap. Such kinetic accelerations allow for tunable and rapid conjugation, reduces the effective concentration of expensively-modified labelling reagents,[14] and provides a simple strategy for multi–component couplings. Initial efforts toward promoting faster cycloaddition kinetics focused on modifications to the cyclooctyne structure, but such strategies experience a problematic trade–off between cyclooctyne reactivity and stability. Benzoannulation of the cyclooctyne ring has furnished rapidly reactive strained–alkyne moieties, such as dibenzocyclooctyne (DBCO) and biarylazacyclooctynone (BARAC), but such rigidified aryl–fused strained–alkynes suffer from poor stability at ambient conditions. To mitigate these limitations, Dommerholt and co–workers developed an aliphatic cyclooctyne bicyclo[6.1.0]nonyne (BCN),[15] that demonstrates exceptional stability and synthetic accessibility, but is kinetically less reactive than its benzoannulated counterparts. Regardless, the superior stability of BCN makes it a more convenient strained–alkyne to work with, compared to DBCO and BARAC.

Contemporary efforts toward enhancing the reaction kinetics of SPAAC/SPANC have converged on structural modifications to the complementary dipolar species. Delocalization of the dipolar species into electron–withdrawing substituents accelerates both SPAAC and SPANC reaction kinetics, while electron–donating substituents decelerate the reaction kinetics.[14,16,17] It should be noted that, unlike SPAAC, an advantageous characteristic of SPANC is that there are three modifiable sites on the nitrone functionality, while terminal azides possess only one modifiable site. Much of the kinetic enhancement of SPANC has been pioneered by Pezacki and co–workers,[14,16] who demonstrated the kinetic consequences of substituent modifications on acyclic nitrones, with their electron–deficient acyclic nitrones having the most accelerated reaction rates. They proceeded to demonstrate that cyclic nitrones possess even greater reaction kinetics through increasing the strain at the nitrone functionality. To the best of our knowledge, the fastest SPANC reaction between a cyclic nitrone and a stable cyclooctyne (BCN) has a bimolecular rate constant (k_2) of 1.5 $M^{-1}s^{-1}$ in methanol.[16]

In order to investigate further acceleration of the SPANC reaction between a nitrone and BCN, we were intrigued by the fastest SPAAC reaction to BCN reported by Dommerholt and co-workers,[17] which occurs between a pyridinium–functionalized azide and BCN ($k_2 = 2.0$ $M^{-1}s^{-1}$ in 9:1 THF:H_2O). We speculated that delocalizing the nitrone moiety into a pyridinium functionality would similarly hasten the SPANC reaction. To that end, we report rapid strain–promoted cycloaddition between a stable cyclooctyne (BCN) and highly electron–deficient nitrones possessing a pyridinium functionality on the nitrone α–carbon. The rapid reactivity of these "pyridinium–nitrones" can be rationalized in terms of favorable energetic overlap between the frontier orbitals of the two reactive partners, that is only observed through inclusion of the pyridinium functionality on the nitrone moiety. To further evaluate the tunability of the reaction kinetics and emphasize the advantageous opportunity for multi–site modifications to nitrones that cannot be achieved with azides, anisole (**3a**), phenyl (**3b**) and benzonitrile (**3c**) substituents were incorporated to the nitrone nitrogen, which results in substantial alterations to the kinetic profiles.

RESULTS AND DISCUSSION

The three pyridinium-nitrones (**3a**–**c**) can be conveniently synthesized in gram–scale quantities using inexpensive, com-

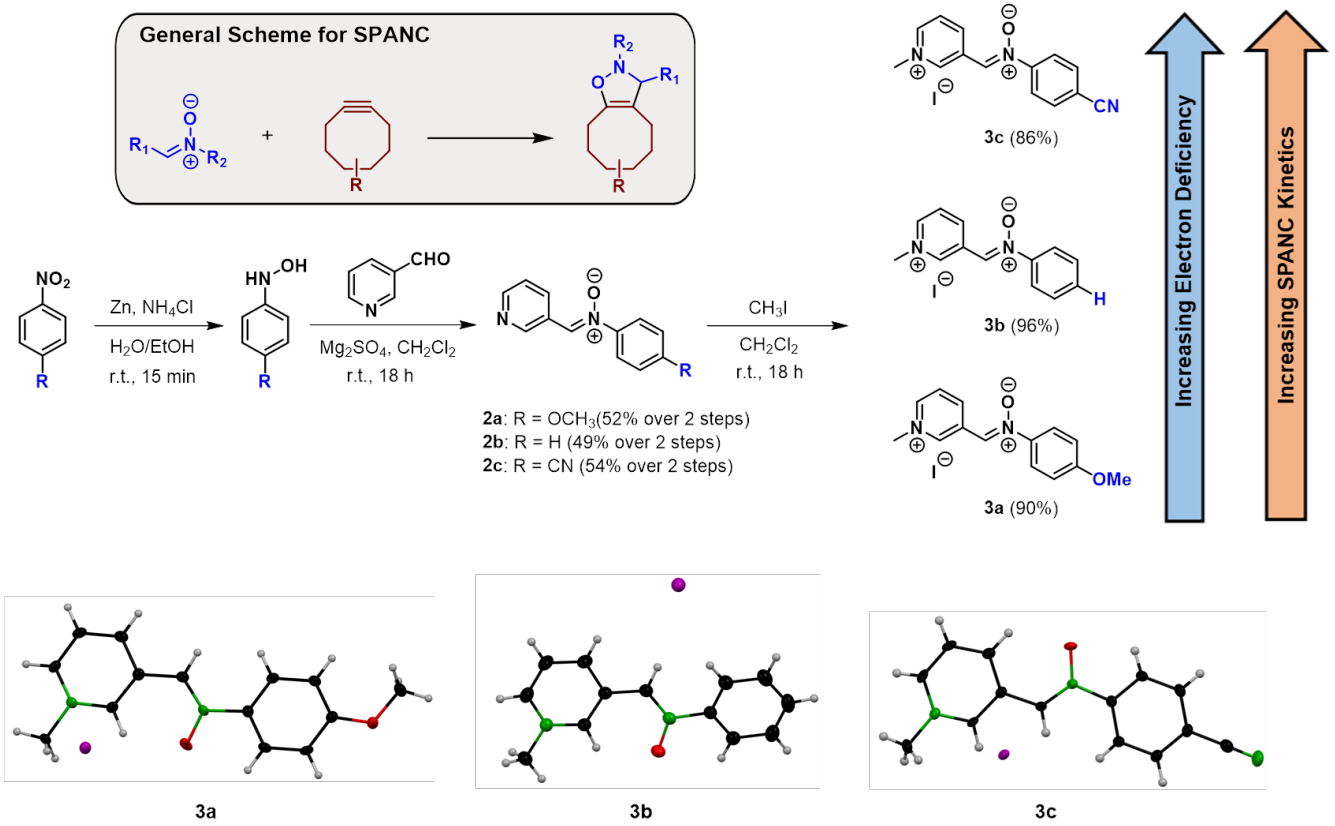

Scheme 1. Synthesis of pyridinium–nitrones possessing anisole (**3a**), phenyl (**3b**) and benzonitrile (**3c**) substituents. Top inset shows general scheme for strain–promoted alkyne–nitrone cycloaddition (SPANC) reaction between nitrone (blue) and cyclooctyne (red). Bottom: molecular structures of **3a**, **3b**, **3c** in the crystal. Thermal ellipsoids are drawn at the 50% probability level with hydrogen atoms drawn with arbitrary radii (black = carbon, red = oxygen, green = nitrogen, purple = iodine)

Table 1. Key parameters of pyridinium–nitrones that vary as electron deficiency (and corresponding reactivity) is increased. ^{1}H NMR spectra were taken in deuterated dimethylsulfoxide at 25°C. Bond lengths were determined from crystallographic data. Mulliken charges (Q) and the energy gap between the HOMO of BCN and LUMO of the nitrone ($\Delta E_{HOMO–LUMO}$) were determined from DFT calculations. Bimolecular rate constants (k_2) were determined under pseudo–first order conditions in 2:1 acetonitrile:tetrahydrofuran at 22°C by UV-Vis spectroscopy.

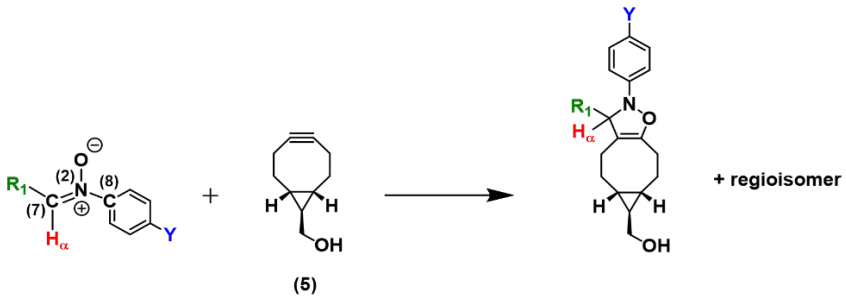

		^{1}H NMR δ of H_α (ppm)	N_2–C_7 Bond Length (Å)	N_2–C_8 Bond Length (Å)	Q at C_7 (a.u.)	ΔE BCN_{HOMO}–$Nitrone_{LUMO}$ (eV)	k_2 ($M^{-1}s^{-1}$)
4	**R_1 = phenyl Y = H**	8.50	1.3126(17)	1.4612(16)	–0.0412	–4.81	0.066 ± 0.004
2b	**R_1 = pyridine Y = H**	8.63	1.3126(12)	1.4555(12)	–0.0360	–4.58	0.15 ± 0.01
3a	**R_1 = pyridinium–CH_3 Y = OCH_3**	8.91	1.305(4)	1.459(4)	–0.0371	–0.532	1.6 ± 0.1
3b	**R_1 = pyridinium–CH_3 Y = H**	8.98	1.3130(15)	1.4607(15)	–0.0302	–0.335	3.3 ± 0.2
3c	**R_1 = pyridinium–CH_3 Y = CN**	9.07	1.314(4)	1.485(4)	–0.0255	–0.0533	8.3 ± 0.3

mercially available reagents and can be purified without the need of chromatography. They are made through condensation of the corresponding hydroxylamine onto 3–pyridinecarboxyaldehyde to generate the pyridine–nitrones (**2a**–**c**) in good yield, which can be subsequently *N*–alkylated using methyl iodide to generate the methylated pyridinium–nitrone species in high yield (**Scheme 1**). Due to the hydrophilicity of the pyridinium functionality, **3a**–**c** are most soluble in polar solvents such as dimethyl sulfoxide, acetonitrile, methanol and water. The characteristic ^{1}H NMR signals of **3a**–**c** are produced by the 2' aromatic proton in the pyridinium ring (**3a** and **3c,** 10.21 ppm and **3b**, 10.23 ppm) and the methyl protons of the pyridinium functionality (**3a,** 4.45 ppm, **3b** and **3c**, 4.46 ppm) (see *Supporting Information*, Section S10). The infrared spectra of **3a**–**c** show a strong band between 1616–1629 cm^{-1} that does not appear in the infrared spectra of **2a**–**c** (see *Supporting Information*, Section S2–S4) and can be assigned to C=N stretching vibrations characteristic of the quaternary nitrogen in the pyridinium ring.[18]

Single crystal X–ray crystallography has been used to verify the structures of **3a**–**c** (see *Supporting Information*, Section S8), which confirms the planarity of the nitrone moiety and aromatic substituents, as well as the trigonal planar geometry of the nitrone moiety. The bond length between the nitrone nitrogen (N_2) and α–carbon (C_7) in **3a**–**c** is consistent with previously reported C=N bond lengths in iminium ions (~1.305Å),[19] which are longer than C=N bond lengths in imines (~1.279Å)[20] due to the larger single bond character in iminium ions. Interestingly, the crystallographic data indicates that there is a slight increase in this N_2–C_7 bond length in **3a**–**c** as increasingly electron–withdrawing substituents are fused to the nitrone moiety (**Table 1**), indicating a weakening of the N_2–C_7 double bond as more electron–withdrawing substituents are fused to the pyridinium–nitrones. Single crystal X-ray crystallography of model compounds **2b** and **4** are included for comparison. The molecular structure of **4** has been reported previously for data collected at room temperature[21], but the data included in Table 1 is measured at 110 K for consistency with the data of **3a-3c.**

The reaction kinetics of **3a**–**c** with BCN-OH_{exo} (**5**) were evaluated under pseudo-first order conditions, according to a previously reported methodology using UV–Vis spectroscopy.[16] A solvent mixture of 2:1 acetonitrile:tetrahydrofuran was used for this study, instead of methanol or water, to minimize any solvent–dependent acceleration in the more polar solvenst that would make measuring the kinetics more difficult. This solvent choice was also chosen to minimize possible hydrolysis of the nitrone, which was observed for **3b** in 6:1 D_2O:$(CD_3)_2SO$ after 12 hours (although **3a** and **3c** were largely unaltered in this solvent after 12 hours) (see *Supporting Information*, Section S16). Rate constants were measured in duplicate at 22°C (**Table 1**) by observing the decrease in absorption at 345 nm produced by the nitrone moiety in **3a**–**c** that is not produced by the resulting isoxazoline product (see *Supporting Information*, Section S17). It should be noted that

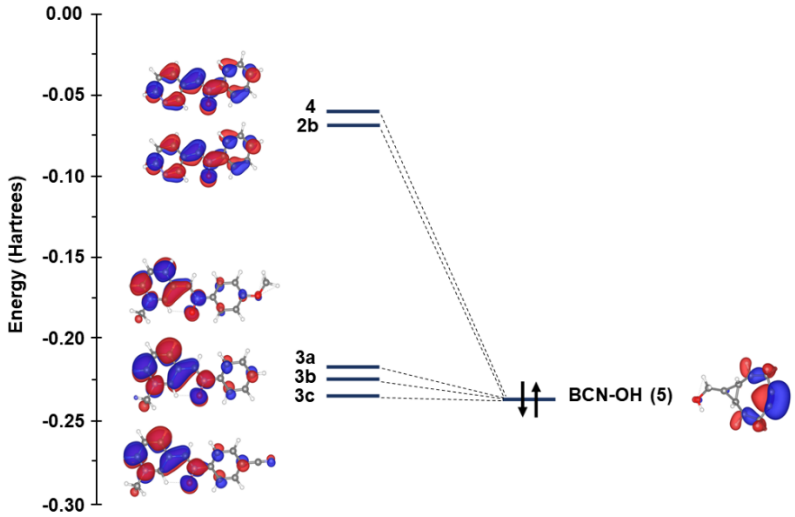

Figure 1. Isosurface plots (isoval = 0.03 e au^{-3}) for the HOMO of BCN–OH$_{exo}$ (**5**) and the LUMO of **3a**–**c**, **4**, **2b**, and energy diagram of the frontier orbitals involved in SPANC between **3a**–**c**, **4**, **2b** and BCN–OH$_{exo}$ (**5**).

the BCN–OH$_{exo}$ isomer was used for this study as it produced in higher quantities during the strained–alkyne synthesis, but the *endo*–isomer can also be used as it would have similar kinetics. Mass spectrometry and NMR spectroscopy (in $(CD_3)_2SO$)) was used to confirm that the pyridinium–nitrones undergoes the SPANC reaction with BCN–OH$_{exo}$ (see *Supporting Information*, section S12). In addition to the three pyridinium–nitrones **3a**–**c**, the rate of reaction for two nitrones delocalized into a phenyl (**4**) and pyridine (**2b**) ring instead of a pyridinium ring was determined, by measuring the decrease in absorption at 316 nm and 320 nm, respectively. Nitrone **4** displayed the slowest rate constant (k_2 = 0.066 M^{-1}s^{-1}) in the series, due to the presence of the least electron-withdrawing α–carbon phenyl and *N*–phenyl substituents. Replacement of the α–carbon phenyl substituent with the more electron–withdrawing α–carbon pyridine substituent in nitrone **2b** results in a two-fold acceleration (k_2 = 0.15 M^{-1}s^{-1}). However, replacement of the α–carbon pyridine with an α–carbon pyridinium ring in **3b** results in an approximate twenty–fold acceleration in the reaction rate (k_2 = 3.3 M^{-1}s^{-1}), which demonstrates the substantial acceleration of SPANC kinetics through pyridinium–conjugation. To illustrate the tunability of SPANC kinetics through the multi–site modification that only exists with SPANC, replacement of the *N*–phenyl substituent in **3b** with a more electron-donating *N*–anisole substituent in **3a** results in an approximate two-fold deceleration of the reaction rate (k_2 = 1.6 M^{-1}s^{-1}). Conversely, exchange of the *N*–phenyl substituent in **3b** with the more electron-withdrawing *N*–benzonitrile substituent in **3c** triggered a significant three–fold acceleration in the reaction rate (k_2 = 8.3 M^{-1}s^{-1}). This is among the fastest click reactions between a dipolar species and BCN reported to date and represents a substantial improvement to the kinetic profile of strain–promoted cycloaddition chemistry.

To illustrate the flexibility of the reaction to solvent choice (that may be applicable for future biological applications), the SPANC reaction between **3c** and BCN–OH$_{exo}$ was successfully carried out and products confirmed by ^{1}H NMR spectroscopy in 6:1 D_2O:$(CD_3)_2SO$, 1:1 D_2O:$(CD_3)_2SO$ and CD_3OD (see *Supporting Information*, section S13). Furthermore, the generality of the reaction between **3c** and different strained alkynes other than BCN–OH$_{exo}$ was probed by challenging **3c** to commercially available dibenzycyclooctyne-amine (DBCO–amine) (see *Supporting Information*, section S14) and a small symmetrical strained–alkyne, (*Z*)–cyclooct–1–ene–5–yne (**6b**) (see *Supporting Information*, section S15). Both SPANC reactions were confirmed by NMR spectroscopy and mass spectrometry.

^{1}H NMR spectroscopy allows for simple, preliminary estimations of nitrone reactivity by comparing the chemical shift of the H$_\alpha$ in the nitrone moiety. As shown in **Table 1**, the H$_\alpha$ in the electron–rich nitrone **3a**, which has the slowest reaction kinetics, appears most upfield at 8.91 ppm. Incorporation of increasingly electron–deficient substituents results in corresponding downfield shifts of the ^{1}H NMR signal of the H$_\alpha$ as the kinetic reactivity is increased, to 8.98 ppm in **3b** and 9.07 ppm in **3c**. Determination of Mulliken atomic charges[22] show that better electron withdrawing groups result in a smaller partial negative charge on the α–carbon (C$_7$) (**Table 1**), which is a consequence of a less electron–rich nitrone moiety and rationalizes the observed deshielding of the H$_\alpha$ as more electron–withdrawing substituents are fused to the pyridinium–nitrone.

The reactivity differences between **3a**–**c** were probed by density functional theory (DFT) computations using the GAUSSIAN09[23] suite of software at the level B3LYP/6–31G*.[24,25] The geometries of the three pyridinium–nitrones were optimized and agree closely with the crystallographic data (see *Supporting Information*, Section S19). The DFT data confirms that, as reported by Dommerholt and co–workers for the SPAAC reaction,[17] the SPANC reaction proceeds via an inverse electron–demand mechanism (IED–SPANC). That is, the frontier orbitals involved in the SPANC reaction are the HOMO of **5**, which is localized mainly on the C–C triple bond, and the LUMO of the pyridinium–nitrones, which is delocalized primarily over the both the nitrone and pyridinium moieties, but also has contributions from the nitrone *N*–substituent (**Figure 1**). Because of these contributions, the energy of the LUMO in IED–SPANC varies according to the electronic nature of the *N*–

substituent on the nitrone moiety, with the electron–donating anisole substituent in **3a** destabilizing the LUMO relative to **3b**, and the electron–withdrawing benzonitrile substituent in **3c** lowering the LUMO energy relative to **3b**. This stabilizing effect results in the convergence of the pyridinium–nitrone LUMO energy level and the HOMO energy level of **5** in the IED–SPANC reaction (**Table 1**). The expected rate enhancement can hence be rationalized in terms of favorable energetic overlap between the two reactants when more electron–withdrawing nitrone *N*–substituents are present. In fact, our DFT calculations indicate that **3c** possesses a miniscule $HOMO_{BCN}$–$LUMO_{nitrone}$ energy gap (–0.0533 eV). This suggests that **3c** is a highly idealized reactive partner for BCN (a stable cyclooctyne), and that any additional tuning to accelerate the reactivity further may provide only small enhancements to the cycloaddition reaction to BCN.

CONCLUSIONS

In conclusion, the incorporation of pyridinium functionalities into nitrone moieties serves as a simple method for substantial acceleration of IED SPANC to BCN. As benzoannulated cyclooctynes are comparatively unstable and expensive to synthesize, it is highly beneficial to utilize more stable aliphatic strained–alkynes like BCN. Furthermore, the acceleration of the cycloaddition reaction serves as an important tool for the efficient conjugation of expensively–modified substrates in chemical biology and nanomaterial sciences to produce reliable and reproducible results at nano– and pico–molar concentrations. It is important to note that our approach not only creates a general method for acceleration of the SPANC reaction, but also incorporates an additional modifiable site: the pyridine functionality. In this prototype study we coupled a methyl group to the pyridine functionality to simplify the analysis. However, given the numerous methodologies for *N*–alkylation of pyridine rings, it should be possible to incorporate the pyridinium–nitrone moiety with alkyl ligands bearing additional functionality for applications using such methodologies, while retaining the rapid kinetics of the pyridinium–nitrone moiety. We are currently exploring such methodologies.

ASSOCIATED CONTENT

Supporting Information

The Supporting Information is available free of charge on the ACS Publications website.

Experimental details of nitrone and strained–alkynes, NMR spectra of nitrones, molecular structures of nitrones determined by X–ray crystallography, NMR spectra of cycloadducts with strained–alkynes, stability tests of nitrones, details of kinetic measurements, summary of crystallographic data and computational details (PDF).

Crystallographic information file (CIF)

AUTHOR INFORMATION

Corresponding Author

* The Department of Chemistry and the Centre for Materials and Biomaterials Research, The University of Western Ontario, Richmond Street, London, Ontario, Canada. E-Mail: mworkent@uwo.ca; Tel: 1 519-661-2111 ext. 86319.

ACKNOWLEDGMENT

The authors would like to thank the National Sciences and Engineering Research Council for financial support of this work, and the University of Western Ontario.

REFERENCES

1. Sletten E.M.; Bertozzi C.R. *Acc. Chem. Res.*, **2011**, *44*, 666.
2. Laughlin S.T.; Baskin J.M.; Amacher S.L.; Bertozzi C.R. *Science*, **2008**, *320*, 664
3. MacKenzie D.A.; Sherratt A.R.; Chigrinova M.; Cheung L.L.W.; Pezacki J.P. *Curr. Opin. Chem. Biol.*, **2014**, *21*, 81.
4. Saxon E.; Bertozzi C.R. *Science*, **2000**, *287*, 2007.
5. Canalle L.A.; van Berkel S.S.; de Haan L.T.; van Hest J.C.M. *Adv. Funct. Mater.*, **2009**, *19*, 3464.
6. Orski S.V.; Poloukhtine A.A.; Arumugam S.; Mao L.D.; Popik V.V.; Locklin J. *J. Am. Chem. Soc.*, **2010**, *132*, 11024.
7. Gobbo P.; Mossman Z.; Nazemi A.; Niaux A.; Biesinger M.C.; Gillies E.R.; Workentin M.S. *J. Mater. Chem. B.*, **2014**, *2*, 1764.
8. Kardelis V.; Chadwick R.C.; Adronov A. *Angew. Chem. Int. Ed.*, **2016**, *55*, 945.
9. Prescher J.A.; Dube D.H.; Bertozzi C.R. Nature, 2004, 430, 873.
10. Sletten E.M.; Bertozzi C.R. *Angew. Chem. Int. Ed.*, **2009**, *48*, 6974.
11. Dommerholt J.; Rutjes F.P.J.T.; van Delft F.L. *Top Curr. Chem. (Z)*, **2016**, *374*, 16.
12. Agard N.J.; Prescher J.A.; Bertozzi C.R. *J. Am. Chem. Soc.*, **2004**, *126*, 15046.
13. Ning X.; Temming R.P.; Dommerholt J.; Guo J.; Ania D.B.; Debets M.F.; Wolfert M.A.; Boons G.-J.; van Delft F.L. *Angew. Chem. Int. Ed.*, **2010**, *49*, 3065.
14. McKay C.S.; Moran J.; Pezacki J.P. *Chem. Commun.*, **2010**, *46*, 931.
15. Dommerholt J.; Schmidt S.; Temming R.; Hendriks L.J.A.; Rutjes F.P.J.T.; van Hest J.C.M.; Lefeber D.J.; Friedl P.; van Delft F.L. *Angew. Chem. Int. Ed.*, **2010**, *49*, 9422.
16. MacKenzie D.A.; Pezacki J.P. *Can. J. Chem.*, **2014**, *92*, 337.
17. Dommerholt J.; van Rooijen O.; Borrmann A.; Guerra C.F.; Bickelhaupt F.M.; van Delft F.L. *Nat. Commun.*, **2014**, *5*, 5738.
18. Spinner E. *J. Am. Chem. Soc.*, **1963**, *0*, 3860.
19. Evans G.J.S.; White K.; Platts J.A.; Tomkinson N.C.O. *Org. Biomol. Chem.*, **2006**, *4*, 2616.
20. Allen F.H.; Kennard O.; Watson D.G. J. Chem. Soc. *Perkin Trans. 2*, **1987**, *0*, S1.
21. (i) Gothelf K.V.; Hazell R.G.; Jorgensen K.A. *Acta. Chem. Scand.*, **1997**, *51*, 1234. (ii) Heinenberg M.; Ritter H.; Schollmeyer. CCDC 813074: Experimental Crystal Structure Determination, **2001**, DOI: 10.5517/ccw926f.
22. Mulliken R.S. *J. Chem. Phys.*, **1955**, *23*, 1833.
23. Frisch M. J.; Trucks G. W.; Schlegel H. B.; Scuseria G. E.; Robb M. A.; Cheeseman J. R.; Scalmani G.; Barone V.; Petersson G. A.; Nakatsuji H.; Li X.; Caricato M.; Marenich A.; Bloino J.; Janesko B. G.; Gomperts R.; Mennucci B.; Hratchian H. P.; Ortiz J. V.; Izmaylov A. F.; Sonnenberg J. L.; Williams-Young D.; Ding F.; Lipparini F.; Egidi F.; Goings J.; Peng B.; Petrone A.; Henderson T.; Ranasinghe D.; Zakrzewski V. G.; Gao J.; Rega N.; Zheng G.; Liang W.; Hada M.; Ehara M.; Toyota K.; Fukuda R.; Hasegawa J.; Ishida M.; Nakajima T.; Honda Y.; Kitao O.; Nakai H.; Vreven T.; Throssell K.; Montgomery, Jr. J. A.; Peralta J. E.; Ogliaro F.; Bearpark M.; Heyd J. J.; Brothers E.; Kudin K. N.; Staroverov V. N.; Keith T.; Kobayashi R.; Normand J.; Raghavachari K.; Rendell A.; Burant J. C.; Iyengar S. S.; Tomasi J.; Cossi M.; Millam J. M.; Klene M.; Adamo C.; Cammi R.; Ochterski J. W.; Martin R. L.; Morokuma K.; Farkas O.; Foresman J. B.; Fox D. J. *Gaussian 09, Revision A.02*, **2016**, Gaussian, Inc., Wallingford CT,.
24. Becke A.D.; *J. Chem. Phys.*, **1993**, *98*, 1372.
25. Lee C.; Yang W.; Parr R.G. *Phys. Rev. B.*, **1988**, *37*, 785